Article

Up-Conversion Luminescence and Temperature Sensing of Er^{3+}/Yb^{3+} Codoped $Y_{2(1-x\%)}Lu_{2x\%}O_3$ Solid Solution

Haoyue Hao, MengYao Zhu, and Liang Li*

Cite This: *ACS Omega* 2023, 8, 6847−6853

Read Online

ACCESS | Metrics & More | Article Recommendations | Supporting Information

ABSTRACT: In this paper, Er^{3+}/Yb^{3+} codoped $Y_{2(1-x\%)}Lu_{2x\%}O_3$ solid solution was prepared through the sol−gel method, and the substitution of Y^{3+} by Lu^{3+} ions in Y_2O_3 was confirmed by X-ray diffraction data. The up-conversion emissions of samples under 980 nm excitation and the relative up-conversion processes are investigated. The emission shapes do not vary with the change in doping concentration due to the unaltered cubic phase. The red-to-green ratio changes from 2.7 to 7.8 and then declines to 4.4 as the doping concentration of Lu^{3+} increases from 0 to 100. The emission lifetimes of green and red have similar variation: the emission lifetime decreases with doping concentration changing from 0 to 60 and rises as the doping concentration continues to increase. The reason why the emission ratio and lifetime change could be originated to the exacerbation of cross-relaxing process and the change of radiative transition probabilities. The temperature-dependent fluorescence intensity ratio (FIR) shows that all samples can be used in noncontact optical temperature sensing, and the method of local structure distortion can be used to improve sensitivity further. The max sensing sensitivities of FIR based on $R_{538/563}$ and $R_{red/green}$ reach 0.011 K^{-1} (483 K) and 0.21 K^{-1} (300 K). The results display that Er^{3+}/Yb^{3+} codoped $Y_{2(1-x\%)}Lu_{2x\%}O_3$ solid solution can be potential candidates for optical temperature sensing in different temperature ranges.
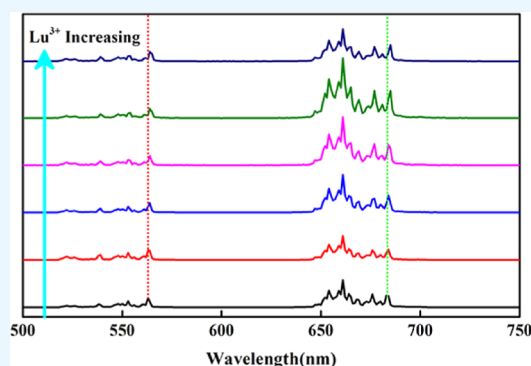
INTRODUCTION

Rare earth ions doped up-conversion materials, possessing optical ability of converting high-energy photons after absorbing multiple low-energy photons, have attracted great attention in many fields, such as colorful display, ion detection, temperature sensing, and so on.[1−5] In temperature sensing, compared with conventional measurement methods like thermocouple and optical fiber, the optical thermometer of rare earth ions doped up-conversion materials shows great advantage for their noninvasive marker. Compared with other optical thermometers, like quantum dots, it possesses merits of nonblinking, low toxicity, and high stability.[6−8] The fluorescence intensity ratio (FIR) technology is regarded as a promising temperature sensing technique because it is impervious to outside interference.[9] The FIR can be calculated through emissions from thermal coupled levels, like green emissions radiated from $^2H_{11/2}/^4S_{3/2}$, or from nonthermal coupled levels, like emissions radiated from $^4F_{9/2}/^2H_{11/2}/^4S_{3/2}$ (Er^{3+}) or $^3F_{2,3}(Tm^{3+})/^4S_{3/2}$ (Er^{3+}).[10−12] The sensing sensitivity based on thermal coupled levels is limited by the restricted energy gap, which is ~200−2000 nm^{-1} and indistinguishable fluorescence spectrum.[13] Therefore, the FIR of emissions from nonthermal coupled levels even from different materials are used to improve the sensitivity.[11,12,14,15] In this work, Er^{3+} is used to emit green and red emissions for temperature sensing. The oxide of rare earth ions is used as host materials for its relative low phonon energy and good chemical stability.[15,16]

The effect of oxide with different crystal phases on up-conversion luminescence and temperature sensing was investigated by Guo' research, which revealed that the sensitivities of the samples were in direct proportion to the local Er^{3+} site symmetry.[16] In addition to crystal phases,[16−18] introducing ions in the host also affects the up-conversion luminescence and sensitivity.[19−21] As discussed in Wang' group, the sensitivity can be improved via inducing Ge ions in $Y_2O_3/Ho^{3+}/Yb^{3+}$ phosphors.[19] The doping concentration was low, and the new phase would appear when a high concentration was introduced.

In this work, we introduce Lu^{3+} into $Y_2O_3/Er^{3+}/Yb^{3+}$ solid solution, where the concentration is 0 to 100% to investigate the influence of local structured distortion on the ratio of red-to-green emissions and the emission lifetime. Meanwhile, the temperature-dependent up-conversion luminescence is detected to evaluate the sensing ability of FIR technology based on thermal coupled levels and noncoupled levels.
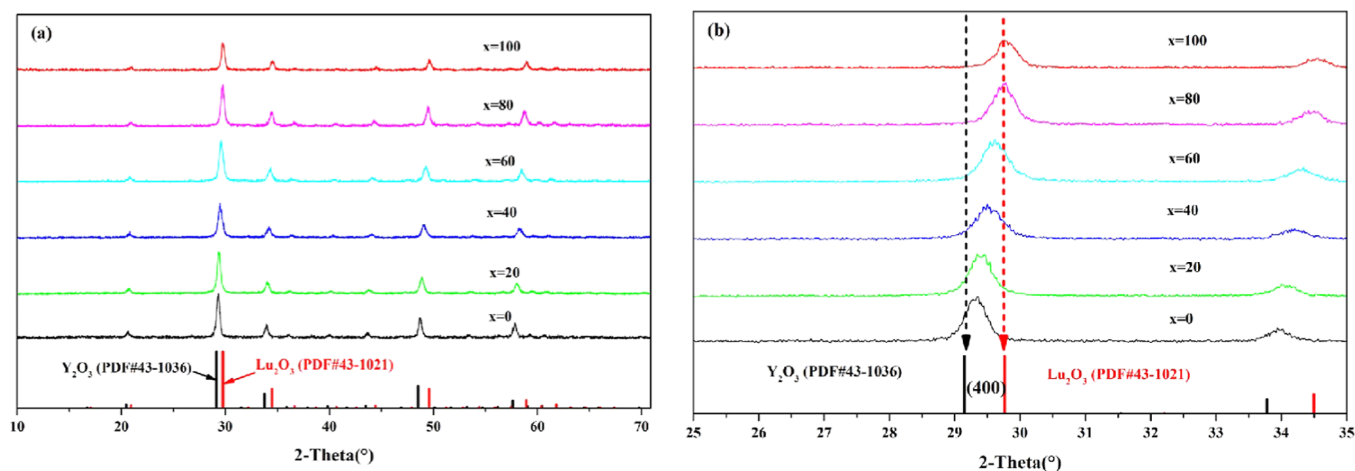
Figure 1. (a) XRD patterns of $Y_{2(1-x\ \%)}Lu_{2(x=0/20/40/60/80/100)\ \%}O_3$ solid solution; (b) enlarged main peaks (400) in all XRD patterns. The black dash line represents the main peaks' position of PDF no. 43-1036; the red dash line represents the main peaks' position of PDF no. 43-1021.
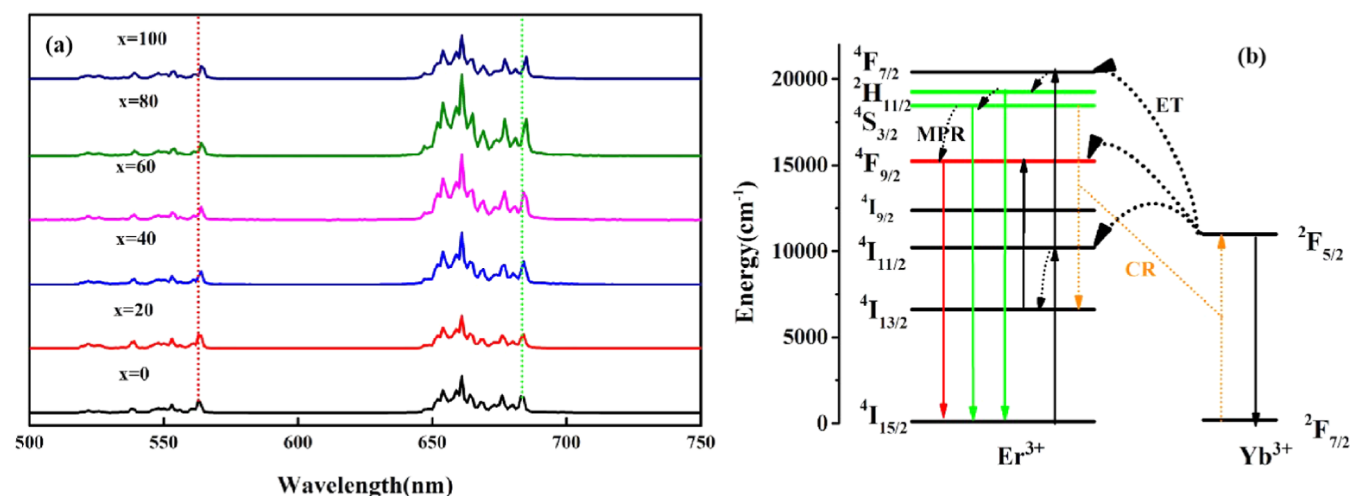

Figure 2. (a) Normalized up-conversion emission in Er^{3+}/Yb^{3+} codoped $Y_{2(1-x\ \%)}Lu_{2x\ \%}O_3$ solid solution (the emission intensities are normalized at 563 nm); (b) schematic energy levels and proposed up-conversion processes of Er^{3+}, Yb^{3+} codoped up-conversion materials.

■ EXPERIMENTAL PART

Materials. $Y(NO_3)_3 \cdot 6H_2O$ (99.9%), $Yb(NO_3)_3 \cdot 6H_2O$ (99.9%), $Er(NO_3)_3 \cdot 6H_2O$ (99.9%), and $Lu(NO_3)_3 \cdot 6H_2O$ (99.9%) were all purchased from Jining Zhongkai New Type Material Science Co., Ltd. $C_6H_8O_7 \cdot H_2O$ (99.5%) was purchased from Aladdin Industrial Corporation. All chemicals were used directly without further purification.

Preparation of Er^{3+}/Yb^{3+} Codoped $Y_{2(1-x\ \%)}Lu_{2x\ \%}O_3$ Solid Solution. In this research, the mole ratio of Er^{3+}/Yb^{3+} in $Y_{2(1-x\ \%)}Lu_{2x\ \%}O_3/Er^{3+}/Yb^{3+}$ solid solution was fixed at 1/4 mol %. The preparation process was as below. Firstl calculated amounts of $Y(NO_3)_3 \cdot 6H_2O$, $Lu(NO_3)_3 \cdot 6H_2O$, $Yb(NO_3)_3 \cdot 6H_2O$, and $Er(NO_3)_3 \cdot 6H_2O$ were dissolved into 10 mL of deionized water and stirred vigorously to form a transparent solution. Meanwhile, calculated amounts of citric acid were dissolved into 10 mL of deionized water. Second, the solution of citric acid was added into the solution of rare earth nitrate dropwise and then agitated for 15 min. The obtained transparent solution was put into a drying oven at 130 °C for 24 h and a muffle furnace at 800 °C for 2 h. The powder was collected after cooling down to room temperature. The values of x were fixed at 0, 20, 40, 60, 80, and 100.

Characterization. In this research, the X-ray diffraction (XRD) patterns of Er/Yb codoped $Y_{2(1-x\ \%)}Lu_{2x\ \%}O_3$ solid solution were measured via an X-ray diffractometer (Empyrean, Panalytical, Netherlands) with Cu Kα radiation ($\lambda = 0.15406$ nm) in the 2θ range from 10 to 70°. The up-conversion spectra of all samples were monitored by the iHR550 grating spectrograph (iHR550, Horiba, France) under 980 nm laser excitation, which was purchased from Beijing Kipling Photoelectric Technology Co., Ltd. For the thermometry experiments, the sample was pasted on a Linkam THMS 600 heating stage and heated. Then, the temperature (T) of the sample was measured by a thermocouple. The spectrum of the sample at a certain temperature (T) was acquired using the iHR550 grating spectrometer. The fluorescence decay curves of the samples were recorded in a DSO5032A digital storage oscilloscope under 980 nm pulse laser excitation.

■ RESULTS AND DISCUSSION

XRD Analysis. The XRD patterns are displayed in Figure 1. As shown in Figure 1a, the XRD patterns of the samples are in good agreement with the standard JCPDS file numbers 43-1036 and 43-1021 when the values of x are 0 and 100, respectively, which is the pure cubic pattern of Y_2O_3 and
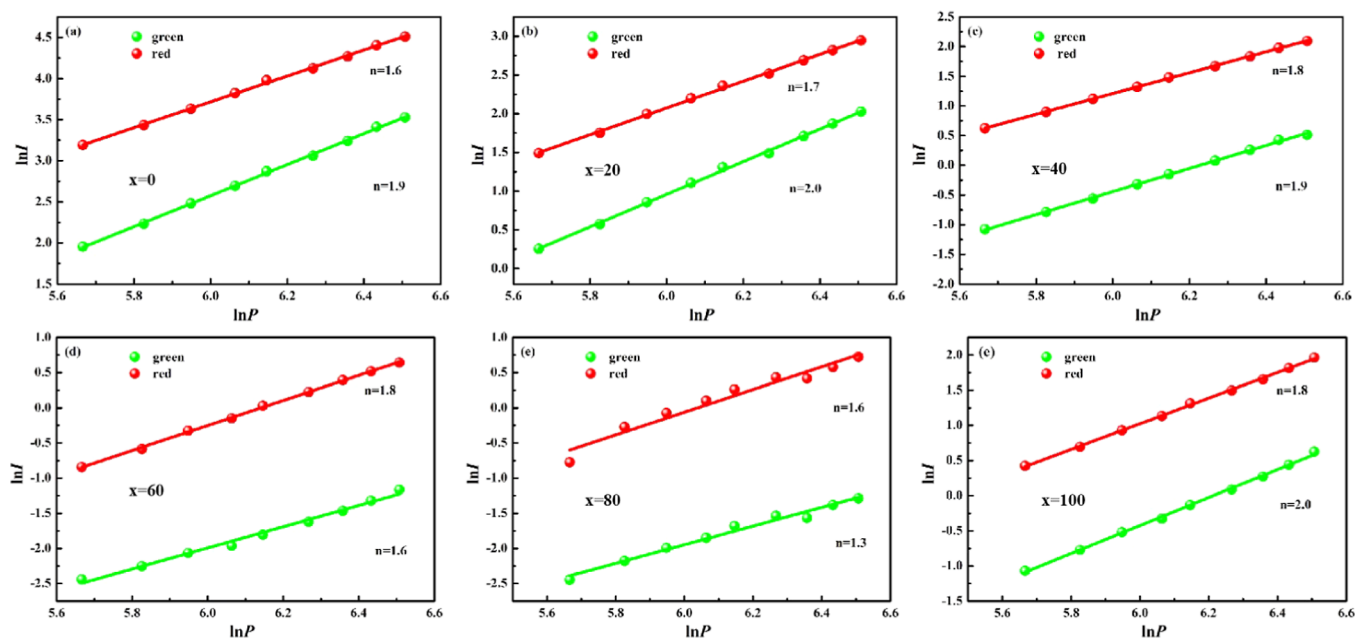
Figure 3. Logarithmic plot of visible emissions versus excitation power of (a) $x = 0$, (b) $x = 20$, (c) $x = 40$, (d) $x = 60$, (e) $x = 80$, and (f) $x = 100$ in Er^{3+}/Yb^{3+} codoped $Y_{2(1-x\%)}Lu_{2x\%}O_3$ solid solution.

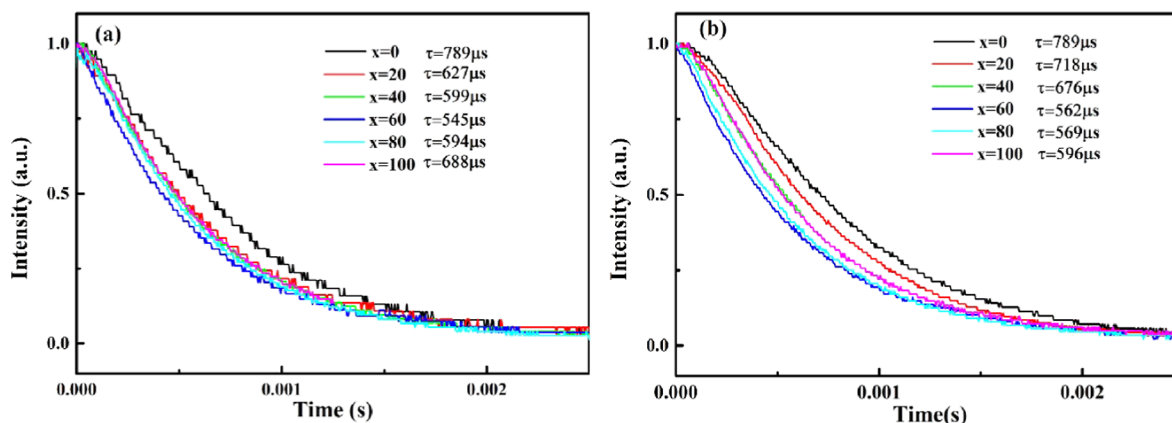**Figure 4.** Decay behaviors of emissions at (a) 563 nm and (b) 661 nm in Er^{3+}/Y^{b3+} codoped $Y_{2(1-x\%)}Lu_{2x\%}O_3$ solid solution.

Lu_2O_3. The strong diffraction peaks of samples are well-consistent with the cubic phase Y_2O_3 and Lu_2O_3 as the value changes from 0 to 100, which indicates that all obtained samples are continuous solid solutions and possess a pure cubic phase structure. This can be attributed to the same charge and similar radius. Moreover, compared with the standard pattern PDF no. 43-1036, an obvious shift toward higher diffraction angles is observed in the enlarged main peak (400) with increasing contents of Lu^{3+} in Y_2O_3 (as shown in Figure 1b), originated to the substitution of Y^{3+} by Lu^{3+} ions with a smaller radius.

Up-Conversion Luminescence Spectra of Er/Yb Codoped $Y_{2(1-x\%)}Lu_{2(x=0/20/40/60/80/100)\%}O_3$ Solid Solution. In order to reveal the effect of doping concentration of Lu^{3+} on the up-conversion luminescence, the up-conversion emission spectra of all samples were detected in the visible region under 980 nm laser excitation. As shown in Figure 2a, typical emissions centered at 538 nm ($^2H_{11/2} \rightarrow {}^4I_{15/2}$), 563 nm ($^4S_{3/2} \rightarrow {}^4I_{15/2}$), and 660 nm ($^4F_{9/2} \rightarrow {}^4I_{15/2}$) can be detected obviously. The spectrum shapes of all powders remain unchanged due to the same space group (la-3(206)), which

was also similar to the spectra of Er^{3+}/Yb^{3+} codoped cubic Gd_2O_3 powder.[22] The emission peaks shift slightly (~1 nm), which can be originated to different crystal-field effects of Y_2O_3 and Lu_2O_3. It is widely accepted that the photons (n), participated in the up-conversion process and can be calculated via the slope of visible emissions versus excitation power. From Figure 3, we can see that the green and red emissions are two typical photon processes of all samples. The detailed up-conversion processes are displayed in Figure 2b. The energy levels, $^2H_{11/2}$ and $^4S_{3/2}$, radiating green emissions, are accumulated through the energy transferred from Yb^{3+} and sequential ground-state absorption ($^4I_{15/2}$ + 980 nm photon $\rightarrow {}^4I_{11/2}$) and excited-state absorption ($^4I_{11/2}$ + 980 nm photon $\rightarrow {}^4F_{7/2}$). The energy levels, $^4F_{9/2}$, radiating red emission, are accumulated through two paths. One is ground-state absorption ($^4I_{15/2}$ + 980 nm photon $\rightarrow {}^4I_{11/2}$), nonradiative transition ($^4I_{11/2} \rightarrow {}^4I_{13/2}$), and excited-state absorption ($^4I_{13/2}$ + 980 nm photon $\rightarrow {}^4F_{9/2}$). The other is multiphonon relaxation from the upper level ($^4S_{3/2}$). The ratios of red-to-green are 2.7, 3.0, 4.7, 8.0, 7.9, and 4.4 as the values of x alter from 0 to 100. The reason why the ratio of red-to-green
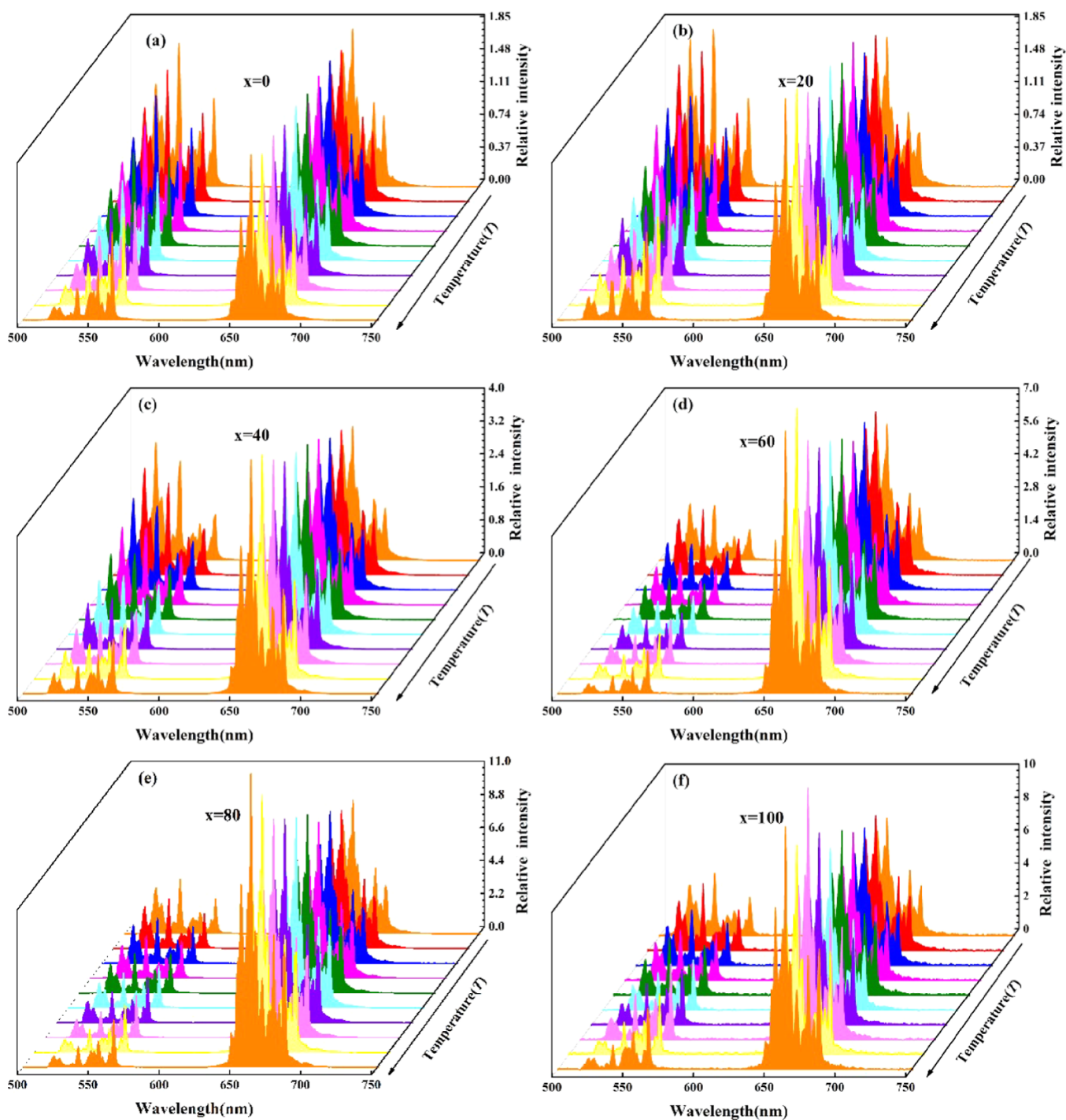
Figure 5. Normalized up-conversion emission of (a) $x = 0$, (b) $x = 20$, (c) $x = 40$, (d) $x = 60$, (e) $x = 80$, and (f) $x = 100$ in Er^{3+}/Yb^{3+} codoped $Y_{2(1-x\%)}Lu_{2x\%}O_3$ solid solution with increasing temperature (emission intensity are normalized at 563 nm).

increases can be explained as follows. As all Y^{3+} ions are replaced by Lu^{3+} ions, the distance between Er^{3+} and Yb^{3+} becomes short for the shorter length of Lu–Lu.d[16] Therefore, the ratio is larger in Er/Yb codoped Lu_2O_3 solid solution due to intense cross-relaxing (CR), as shown in Figure 2b. As a part of Y^{3+} ions are replaced by Lu^{3+} ions, the local structural distortion is generated and could induce intense CR between Er^{3+} and Yb^{3+}. The local structure distortion may also cause a change in the radiative transition probabilities of $^2H_{11/2}/^4S_{3/2} \rightarrow {}^4I_{15/2}$ and $^4F_{9/2} \rightarrow {}^4I_{15/2}$ transitions.[23,24] Hence, the ratios of red-to-green are strongly affected by local structural distortion.

Figure 4 shows the decay curves of 563 and 661 nm emissions from Er^{3+}/Yb^{3+} doped $Y_{2(1-x)}Lu_{2(x=0/20/40/60/80/100)\%}O_3$ solid solution. The emission lifetimes (τ) are calculated through single exponential decay function, and the detailed emission lifetimes are displayed in Figure 4. The emission lifetime decreases first and then increases as the doping concentration of Lu^{3+} changes from 0 to 100. The reason could also be originated to the change of CR process and the radiative transition probabilities of $^2H_{11/2}/^4S_{3/2} \rightarrow {}^4I_{15/2}$ and $^4F_{9/2} \rightarrow {}^4I_{15/2}$ transitions.
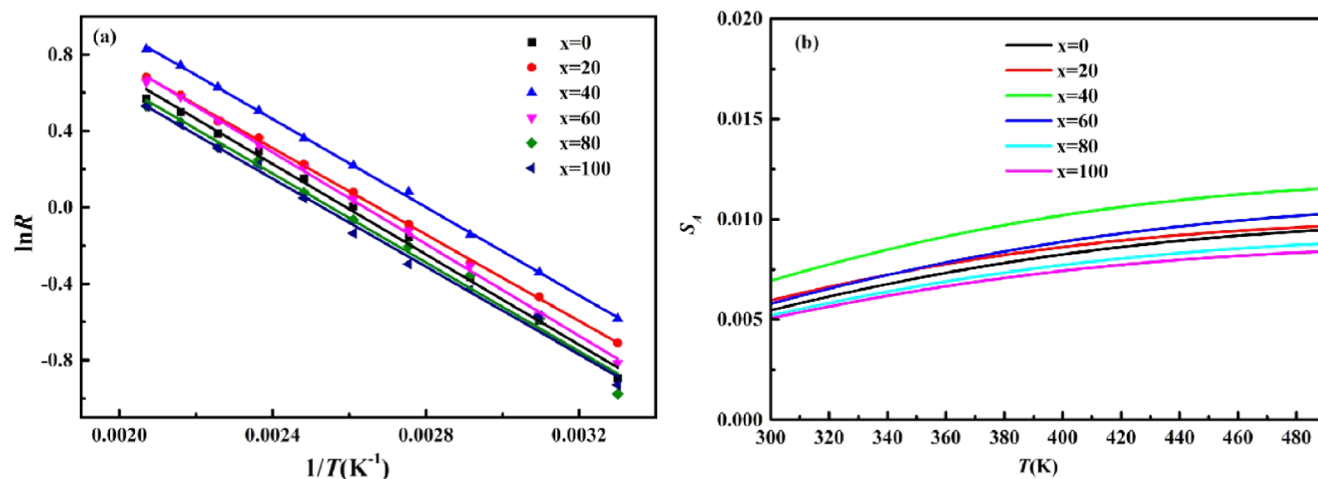
Figure 6. (a) Temperature-dependent $\ln R_{538/563}$ and (b) S_A.

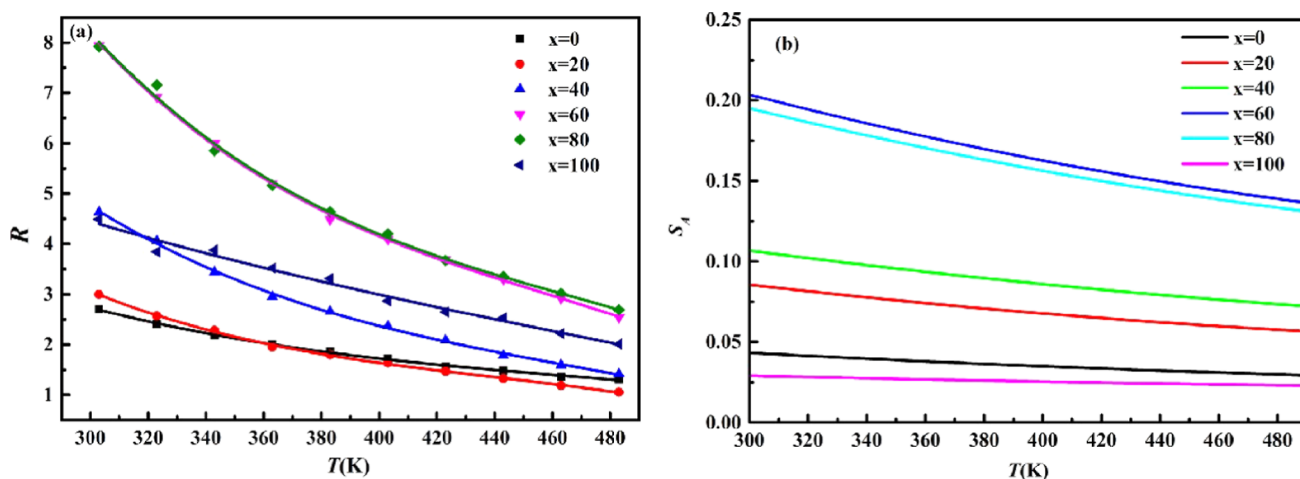**Figure 7.** (a) Temperature-dependent $R_{red/green}$ and (b) S_A.

Temperature-Dependent Up-Conversion Luminescence of Er^{3+}/Yb^{3+} Codoped Y$_{2(1-x\%)}$Lu$_{2x\%}$O$_3$ Solid Solution. To evaluate the capability of temperature sensing in Er^{3+}/Yb^{3+} codoped Y$_{2(1-x\%)}$Lu$_{2x\%}$O$_3$ solid solution, we study the temperature-dependent up-conversion luminescence (from 500 to 750 nm) of all samples. The temperature-dependent emission spectra with temperature varying from 303 to 483 K are displayed in Figure 5. The emission intensities are normalized at 563 nm to show the variation tendency of two green emissions (located in the wavelength range of 500 to 543 and 543 to 580 nm). As can be shown in Figure 5, the emission locations do not move with temperature increasing, and the green emission intensity (I_{538}) increases as the temperature increases because of thermal excitation.[25,26] Thus, the ratio of two green emissions located at 538 and 563 nm are calculated for their superior thermal coupled ability. The FIR can be expressed as eqs 1 and 2 because the population of thermal coupled levels follows the Boltzmann distribution. In eq 1, R stands for FIR, and I_{538} and I_{545} are the integrated intensities of green emissions. ΔE is the energy gap between energy levels $^2H_{11/2}$ and $^4S_{3/2}$, C is the constant related to degeneracy, radiative transition probability, and angular frequency. T is the absolute temperature. Equation 1 can be modified to eq 2 to see the fitting line visibly. The

absolutely sensitivity can be calculated through eq 3 to indicate the temperature-sensing ability.

$$R = \frac{I_{538}}{I_{563}} = C \exp\left(-\frac{\Delta E}{kT}\right) \tag{1}$$

$$\ln R = -a/T + b \tag{2}$$

$$S_A = \left|\frac{dR}{dT}\right| = \frac{a}{T^2} e^{bT - a/T} \tag{3}$$

The relationships between $\ln R$ and $1/T$ of Y$_{2(1-x\%)}$Lu$_{2(x=0/20/40/60/80/100)\%}O_3$ solid solution are shown in Figure 6a. The data of $\ln R$ can be fitted well with linear functions, and the fitted parameters are displayed in Table S1. The values of R-square are less than 0.99. Therefore, the ratio of two green emissions can be used to sense temperature via noncontact FIR method. The absolutely sensitivity, calculated through eq 3, is plotted in Figure 6b. The maximum sensing sensitivity reaches 0.011 K^{-1} at 483 K when the value of x is equal to 40. The result indicates that sensing sensitivity can be improved when a certain amount of Lu^{3+} is doped in Y$_2$O$_3$, which could be originated to the dopant-induced local structural distortion. What is more, the sensing sensitivity can further improve through the FIR of sublevel from $^2H_{11/2}$ and $^4S_{3/2}$.[22]

In order to improve the sensing sensitivity, the noncontact optical temperature sensing based on the FIR of nonthermal coupled levels is investigated. The ratio of red-to-green ($R_{\text{red/green}}$) is shown in Figure 7a. For nonthermal coupled levels, the temperature-dependent $R_{\text{red/green}}$ is typically fitted by a polynomial.[27] Therefore, we fitted the temperature-dependent $R_{\text{red/green}}$ through a cubic function $R = B_0 + B_1 T + B_2 T^2 + B_2 T^3$, and the fitted values are displayed in Table S2. The data of $R_{\text{red/green}}$ are fitted well with cubic functions, and the values of R-square are less than 0.99. To investigate the sensing abilities of different samples, we calculated the absolute sensing sensitivity (S_a) through the expression $S_a = |dR/dT|$. The sensitivities of samples are shown in Figure 7b. The maximum value of S_a reaches 0.21 K^{-1} (300 K) in Y$_{2(1-x\%)}$Lu$_{2(x=60)\%}$O$_3$ solid solution. The sensitivities of nonthermal levels from all samples are higher than those of thermal levels and can be used in fields like surface temperature imaging. As shown in Figure 6b, the sensing sensitivity of $R_{538/563}$ increases as the temperature rises, indicating its potential application in the high-temperature range. The sensing sensitivity decreases with increase in temperature (Figure 7b), which implies that temperature sensing based on nonthermal coupled levels can be utilized in biological application. Compared with other works, the samples in this work exhibits higher temperature sensitivity and can be applied in sensing devices to detect temperature in high- or low-temperature range.[28−31]

CONCLUSIONS

In summary, the up-conversion luminescence and the temperature-sensing ability of cubic-phased Er^{3+}/Yb^{3+} codoped Y$_{2(1-x\%)}$Lu$_{2x\%}$O$_3$ solid solution were investigated. The emission shape does not vary with the change of Lu^{3+} concentration. The emission locations shifted to longer wavelength (∼1 nm), which could be due to different crystal-field effects of Y$_2$O$_3$ and Lu$_2$O$_3$. The red-to-green ratio changes from 2.7 to 8.0 and then declines to 4.4 as the doping concentration of Lu^{3+} increases from 0 to 100. The emission lifetimes of green and red emissions have similar variation: the emission lifetime decreases with doping concentration changing from 0 to 60 and rises as the doping concentration continues to increase. The reason for the change in the emission ratio and lifetime could be originated to the transition of CR process and the change of radiative transition probabilities. The temperature-dependent up-conversion luminescence shows that all samples can be used in noncontact optical temperature sensing. The max sensing sensitivities of FIR based on $R_{538/563}$ and $R_{\text{red/green}}$ reach 0.011 K^{-1} (483 K) and 0.21 K^{-1} (300 K). The calculated sensing sensitivities display that local structural distortion, induced by doping Lu^{3+}, can further improve sensing sensitivity.

ASSOCIATED CONTENT

Supporting Information

The Supporting Information is available free of charge at https://pubs.acs.org/doi/10.1021/acsomega.2c07565.

> Fitted parameters in FIR thermometry (based on R538/563) from different samples and fitted parameters in FIR thermometry (based on Rred/green) from different samples (PDF)

AUTHOR INFORMATION

Corresponding Author

Liang Li − School of Physics and Optoelectronic Engineering, Shandong University of Technology, Zi Bo 255000, China; orcid.org/0000-0003-0270-8080; Email: liangli@sdut.edu.cn

Authors

Haoyue Hao − School of Physics and Optoelectronic Engineering, Shandong University of Technology, Zi Bo 255000, China; orcid.org/0000-0002-4251-4064

MengYao Zhu − School of Physics and Optoelectronic Engineering, Shandong University of Technology, Zi Bo 255000, China

Complete contact information is available at:
https://pubs.acs.org/10.1021/acsomega.2c07565

Author Contributions

H.H. conceived, designed, and carried out the experiments, analyze data, and wrote the paper. M.Z. took the spectra. L.L. supports the devices.

Notes

The authors declare no competing financial interest.

REFERENCES

(1) Jia, H.; Li, D.; Zhang, D.; Dong, Y.; Ma, S.; Zhou, M.; Di, W.; Qin, W. High Color-Purity Red, Green, and Blue-Emissive Core-Shell Upconversion Nanoparticles Using Ternary Near-Infrared Quadrature Excitations. *ACS Appl. Mater. Interfaces* **2021**, *13*, 4402−4409.

(2) Yang, X.; Zhang, Y.; Zhang, P.; He, N.; Yang, Q.; Peng, H.; Zhai, B.; Gui, J. pH Modulations of Fluorescence LaVO$_4$: Eu^{3+} Materials with Different Morphologies and Structures for Rapidly and Sensitively Detecting Fe^{3+} ions. *Sens. Actuators, B* **2018**, *267*, 608−616.

(3) Huang, F.; Yang, T.; Wang, S.; Lin, L.; Hu, T.; Chen, D. Temperature Sensitive Cross Relaxation between Er^{3+} Ions in Laminated Hosts: A Novel Mechanism For Thermochromic Upconversion and High Performance Thermometry. *J. Mater. Chem. C* **2018**, *6*, 12364−12370.

(4) Chen, G.; Ågren, H.; Ohulchanskyy, T. Y.; Prasad, P. N. Light Upconverting Core-Shell Nanostructures: Nanophotonic Control for Emerging Applications. *Chem. Soc. Rev.* **2015**, *44*, 1680−1713.

(5) Zhang, Z.; Shikha, S.; Liu, J.; Zhang, J.; Mei, Q.; Zhang, Y. Upconversion Nanoprobes: Recent Advances in Sensing Applications. *Anal. Chem.* **2018**, *91*, 548−568.

(6) Bednarkiewicz, A.; Marciniak, L.; Carlos, L. D.; Jaque, D. Standardizing Luminescence Nanothermometry for Biomedical Applications. *Nanoscale* **2020**, *12*, 14405−14421.

(7) Xiao, Q.; Yin, X.; Dong, X.; Zhou, N.; Wang, Y.; Zhang, X.; Luo, X.; Song, Y. High-Sensitive Temperature Sensing Based on Thermal-Enhanced Emission and Non-thermally Coupled Energy Levels of White Upconversion Luminescence System. *Spectrochim. Acta, Part A* **2022**, *281*, 121608.

(8) Runowski, M.; Stopikowska, N.; Szeremeta, D.; Goderski, S.; Skwierczyńska, M.; Lis, S. Upconverting Lanthanide Fluoride Core@Shell Nanorods for Luminescent Thermometry in the First and Second Biological Windows: β-NaYF$_4$: Yb^{3+}-Er^{3+}@SiO$_2$ Temperature Sensor. *ACS Appl. Mater. Interfaces* **2019**, *11*, 13389−13396.

(9) Brites, C. D.; Lima, P. P.; Silva, N. J.; Millán, A.; Amaral, V. S.; Palacio, F.; Carlos, L. D. Thermometry at the Nanoscale. *Nanoscale* **2012**, *4*, 4799−4829.

(10) Ma, Z.; Gou, J.; Zhang, Y.; Man, Y.; Li, G.; Li, C.; Tang, J. Yb^{3+}/Er^{3+} Co-Doped Lu$_2$TeO$_6$ Nanophosphors: Hydrothermal Synthesis, Upconversion Luminescence and Highly Sensitive Temperature Sensing Performance. *J. Alloys Compd.* **2019**, *772*, 525−531.

(11) Lu, H.; Hao, H.; Shi, G.; Gao, Y.; Wang, R.; Song, Y.; Wang, Y.; Zhang, X. Optical Temperature Sensing in β-NaLuF$_4$: Yb^{3+}/Er^{3+}/Tm^{3+} based on Thermal, Quasi-thermal and Non-thermal Coupling Levels. *RSC Adv.* **2016**, *6*, 55307−55311.

(12) Han, Q.; Hao, H.; Yang, J.; Sun, Z.; Sun, J.; Song, Y.; Wang, Y.; Zhang, X. Optical Temperature Sensing Based on Thermal, Non-Thermal Coupled Levels and Tunable Luminescent Emission Colors of Er^{3+}/Tm^{3+}/Yb^{3+} tri-doped Y$_7$O$_6$F$_9$ Phosphor. *J. Alloys Compd.* **2019**, *786*, 770−778.

(13) Du, P.; Luo, L.; Huang, X.; Yu, J. S. Ultrafast Synthesis of Bifunctional Er^{3+}/Yb^{3+}-Codoped NaBiF$_4$ Upconverting Nanoparticles for Nanothermometer and Optical Heater. *J. Colloid Interface Sci.* **2018**, *514*, 172−181.

(14) Stopikowska, N.; Runowski, M.; Skwierczyńska, M.; Lis, S. Improving Performance of Luminescent Nanothermometers based on Non-Thermally and Thermally Coupled Levels of Lanthanides by Modulating Laser Power. *Nanoscale* **2021**, *13*, 14139−14146.

(15) Avram, D.; Colbea, C.; Florea, M.; Tiseanu, C. Highly-Sensitive Near Infrared Luminescent Nanothermometers Based on Binary Mixture. *J. Alloys Compd.* **2019**, *785*, 250−259.

(16) Suo, H.; Zhao, X.; Zhang, Z.; Shi, R.; Wu, Y.; Xiang, J.; Guo, C. Local Symmetric Distortion Boosted Photon Up-Conversion and Thermometric Sensitivity in Lanthanum Oxide Nanospheres. *Nanoscale* **2018**, *10*, 9245−9251.

(17) Chen, D.; Wan, Z.; Zhou, Y.; Zhou, X.; Yu, Y.; Zhong, J.; Ding, M.; Ji, Z. Dual-Phase Glass Ceramic: Structure, Dual-Modal Luminescence, and Temperature Sensing Behaviors. *ACS Appl. Mater. Interfaces* **2015**, *7*, 19484−19493.

(18) Li, D.; Xu, W.; Huang, Z.; Jin, X.; Xu, B.; Zhang, Z.; Zhang, T.; Wang, D.; Liu, X.; Suo, H.; Li, Q. Simultaneous Enhancement of Emission and Thermal Sensitivity via Phase Transition in Gd$_2$(MoO$_4$)$_3$:Yb^{3+}/Er^{3+} Crystals. *J. Am. Ceram. Soc.* **2022**, *106*, 438−447.

(19) Kumar, V.; Zoellner, B.; Maggard, P. A.; Wang, G. Effect of Doping Ge into Y$_2$O$_3$:Ho,Yb on the Green-to-Red Emission Ratio and Temperature Sensing. *Dalton Trans.* **2018**, *47*, 11158−11165.

(20) Jin, Y.; Pang, T. Highly Efficient Green Upconversion Luminescence of ZnMoO$_4$: Yb^{3+}/Er^{3+}/Li$^+$ for Accurate Temperature Sensing. *Spectrochim. Acta, Part A* **2019**, *211*, 306−312.

(21) Lu, H.; Hao, H.; Zhu, H.; Shi, G.; Fan, Q.; Song, Y.; Wang, Y.; Zhang, X. Enhancing Temperature Sensing Behavior of NaLuF$_4$:Yb^{3+}/Er^{3+} via Incorporation of Mn^{2+} Ions Resulting in a Closed Energy Transfer. *J. Alloys Compd.* **2017**, *728*, 971−975.

(22) Hao, H.; Zhang, X.; Wang, Y.; Liang, L. Color Modulation and Temperature Sensing Investigation of Gd$_2$O$_3$:1 mol% Er^{3+}, 1 mol% Yb^{3+} Phosphors under Different Excitation Condition. *J. Lumin.* **2019**, *215*, 116556.

(23) Pang, T.; Wu, Y.; Zhang, Y.; Jian, R.; Mao, J.; Wang, H.; Guo, H. Excitation-wavelength-dependent anti-thermal quenching of upconversion luminescence in hexagonal NaGdF$_4$: Nd^{3+}/Yb^{3+}/Er^{3+} nanocrystals. *J. Mater. Chem. C* **2022**, *10*, 5109−5115.

(24) Pang, T.; Jian, R.; Mao, J.; Guo, H. Improved Response of Upconversion Luminescence Color to Pump Power through the Coupling of Er^{3+} and Tm^{3+}. *J. Phys. Chem. C* **2022**, *126*, 1481−1488.

(25) Du, P.; Su Yu, J. S. Effect of molybdenum on upconversion emission and temperature sensing properties in Na$_{0.5}$Bi$_{0.5}$TiO$_3$:Er/Yb ceramics. *Ceram. Interfaces* **2015**, *41*, 6710−6714.

(26) Chen, Y.; Chen, G. H.; Liu, X. Y.; Yang, T. Enhanced Up-Conversion Luminescence and Optical Thermometry Characteristics of Er^{3+}/Yb^{3+} Co-Doped Transparent Phosphate Glass-Ceramics. *J. Lumin.* **2018**, *195*, 314−320.

(27) Lu, H.; Hao, H.; Gao, Y.; Li, D.; Shi, G.; Song, Y.; Wang, Y.; Zhang, X. Optical Sensing of Temperature Based on Non-Thermally Coupled Levels and Upconverted White Light Emission of a Gd$_2$(WO$_4$)$_3$ Phosphor Co-Doped with in Ho(III), Tm(III), and Yb(III). *Microchim. Acta* **2017**, *184*, 641−646.

(28) Singh, P.; Jain, N.; Tiwari, A. K.; Shukla, S.; Baranwal, V.; Singh, J.; Pandey, A. C. Near-Infrared Light-Mediated Er^{3+} and Yb^{3+} Co-Doped CaTi$_4$O$_9$ for Optical Temperature Sensing Behavior. *J. Lumin.* **2021**, *233*, 117737.

(29) Pavani, K.; do Nascimento, J. P. C.; Jakka, S. K.; do Carmo, F. F.; Sales, A. J. M.; Soares, M. J.; Graça, M. P. F.; de Aquino, F. J. A.; Gouveia, D. X.; Sombra, A. S. Analogy of Different Optical Temperature Sensing Techniques in LaNbO$_4$: Er^{3+}/Yb^{3+} Phosphor. *J. Lumin.* **2021**, *235*, 117992.

(30) Ran, W.; Sun, G.; Ma, X.; Zhang, Z.; Yan, T. Excellent Up Conversion Luminescence and Temperature Sensing Performance of CdMoO$_4$: Er^{3+}, Yb^{3+} Phosphor. *Dalton Trans.* **2022**, *51*, 8749−8756.

(31) Chen, G.; Lei, R.; Huang, F.; Wang, H.; Zhao, S.; Xu, S. Optical Temperature Sensing Behavior of Er^{3+}/Yb^{3+}/Tm^{3+}:Y$_2$O$_3$ Nanoparticles Based on Thermally and Non-Thermally Coupled Levels. *Opt. Commun.* **2018**, *407*, 57−62.